Tribology Letters (2024) 72:32
https://doi.org/10.1007/s11249-023-01827-z

ORIGINAL PAPER

Clarification of the Effect of Surface Energy on Tribological Behavior of Two-Phase Lubricant Using Reflectance Spectroscopy and Hydrodynamic Analysis

Kodai Hirata[1] · Motoyuki Murashima[2] · Noritsugu Umehara[1] · Takayuki Tokoroyama[1] · Woo-Young Lee[3] · Naoya Hashizume[1] · Taku Sato[4] · Ryoko Nagata[4] · Kiyoshi Hanyuda[4] · Ayano Otsuka[4] · Mao Ueda[4]

Received: 11 October 2023 / Accepted: 31 December 2023 / Published online: 13 February 2024

Abstract

Recently, a new type of lubricant called two-phase lubricants has been developed to realize a high viscosity index. Two-phase lubricants are mixtures of two different lubricants, realizing low viscosity even at low temperatures due to the temperature dependence of the solubility of the lubricant molecules. In the present paper, the effect of surface energy on the tribological behavior of the two-phase lubricant is clarified using in situ observation with reflection spectroscopy. Sliding surfaces with high hydrogen-bonding terms in the surface energy components attracted high-polar lubricants, resulting in reduced friction. Analysis of the theoretical friction coefficient using Couette flow assumption revealed an important design concept of two-phase lubricants: the concentration of high viscosity lubricants on solid surfaces develops a viscosity distribution in the oil film, resulting in reduced friction.

Keywords Two-phase lubricant · In situ reflectance spectroscopy observation · Surface energy · Hydrodynamic lubrication

List of Symbols

θ_{SL}	Contact angle between droplet and disk
x	Droplet height
Y	Droplet width
γ	Surface energy (Subscript L and S are liquid and solid, respectively. Superscript h and d are hydrogen-bonding force and dispersion force, respectively)
R	Reflectance measured by reflectance spectroscopy
$R_{01234567}$	Theoretical reflectance calculated by optical model
r_{ij}	The amplitude reflectivity between the interface of i and j
β_m	The interference phase angle of mth layer
N_m	Complex reflective index of mth layer
n_m	Reflective index of mth layer
k_m	Extinction coefficient of mth layer
t_m	Thickness of the mth layer in the optical model
θ_m	Incident angle of light entering the m-th layer
λ	Wavelength
c_k	Volumetric concentration of colored PAG in oil film layer
$\varepsilon_{mineral}oil$	Dielectric constant of mineral oil
$\varepsilon_{coloured}PAG$	Dielectric constant of colored PAG
ε_k	Dielectric constant of oil film layer
h_1, h_2, h_3	Oil film thickness of each layer
μ_{ex}	Experimental friction coefficient
v_{1h}, v_{2h}, v_{3h}	Velocity gradient of the lubricant in each layer $\left(=\frac{\partial v_k}{\partial h}\right)$
V	Sliding speed of friction test
τ_1, τ_2, τ_3	Shear stress on the lubricant in each layer

✉ Motoyuki Murashima
motoyuki.murashima.b3@tohoku.ac.jp

[1] Department of Micro-Nano Mechanical Science and Engineering, Nagoya University, Furo-cho, Chikusa-ku, Nagoya City, Aichi 464-8603, Japan

[2] Department of Mechanical Systems Engineering, Tohoku University, 6-6-01 Aoba, Aramaki, Aoba-ku, Sendai, Miyagi 980-8579, Japan

[3] Intelligent Optical Module Research Center, Korea Photonics Technology Institute, Cheomdan Venture-ro 108-Gil 9, Buk-gu, Gwangju 61007, Republic of Korea

[4] Technology Centre Research & Development Team, Shell Lubricants Japan K.K, Nakatsu Aikawa-Machi, Aiko-gun, Kanagawa 243-0303, Japan

α	Viscosity-pressure coefficient
p_{mean}	Mean Hertzian contact pressure during friction test
μ_{th}	Theoretical friction coefficient
A	Hertzian contact area
c_{mean}	Mean volumetric concentration of colored PAG in the whole oil film

1 Introduction

Currently, there is a strong demand to improve the energy efficiency of automobile engines in order to reduce carbon dioxide emissions. Since friction losses account for 16.5% of the energy input to automobiles, reducing friction losses is an important issue [1]. There are some techniques to reduce friction loss in the internal combustion engines. One common method is applying functional coatings on the surfaces. Recently, DLC (diamond-like carbon) coatings have attracted much attention due to advantageous properties including low friction [2–5], high hardness [6–8], wear resistance [9–15], and chemical stability [16–18]. Early studies showed that DLC coatings exhibit very low friction in dry conditions [19–31], but in recent years, many studies have demonstrated low friction and anti-wear characteristics in oil lubrication conditions [32–41]. Due to the excellent tribological characteristics of DLC coatings, some engines already have DLC-coated components [42–46]. Surface morphology and texturing effects have also been studied in terms of their influence on the friction and adhesion [47–51]. It has been found that micro/nano-scale texturing improves the lubrication condition, causing less hydrodynamic loss in the tribosystem [52, 53]. More recently, new morphing surfaces and machine learning have been combined to control friction [54].

The lubricant itself is also an important component in reducing frictional losses in engine system. There are two main components determining performance of an engine oil; one is the additives in the oil and the other is the type of base oil. Each additive has its own role in influencing tribological performance (e.g., viscosity index improvers, anti-foaming agents, anti-wear additives, extreme-pressure agents, and friction modifiers: the latter two are very important in the field of tribology [55–65]). For example, MoDTC (molybdenum dithiocarbamate) and ZnDTP (zinc dialkyldithiophosphate) [59, 66] have been actively studied to achieve low friction loss and long engine life. Several simulations showed that wear and stress due to external forces (e.g., friction) can cause changes in electron density [67–69], and these effects are thought to contribute to the adsorption of molecules and the formation of additive-derived tribofilms[70, 71]. Most tribology researches on engine oils have focused on the effects of additives, but recently the concept of two-phase lubrication has been gaining attention.

Generally, low viscosity oils are used to reduce engine friction losses. Recently, 0W-20, a superlow viscosity grade, has become the mainstream engine oil [72–74]. However, low viscosity oil has the disadvantage that its viscosity drops drastically as temperature rises. As a result of the significant drop in viscosity, lubrication conditions become very severe, causing severe wear and increased friction.

A new type of lubricant, called two-phase lubricant, has the potential to overcome the drawback of low viscosity oils [75]. The two-phase lubricant consists of a semi-miscible state of two oils of low and high viscosity. At low temperatures, the two-phase lubricant is highly separated into the high viscosity oil and the low viscosity oil. At this time, the high viscosity oil accumulates at the bottom of the oil pan in the engine system due to its large molecular weight and high fluid resistance. As a result, the characteristics of the low viscosity oil dominate the function of the lubricant at low temperatures. As the engine temperature rises, the high viscosity oil dissolves into the low viscosity oil, preventing excessive viscosity reduction. As a result, two-phase lubricants can achieve excellent viscosity indexes. Recently proposed two-phase lubricants consist of a non-polar low viscosity oil (PAO or mineral oil) and a high viscosity polyalkylene glycol (PAG) with polar functional groups. Kamata et al. measured the viscosity index of two-phase lubricants and found that the viscosity index of two-phase lubricants ranged from 400 to 700, higher than 200 for conventional engine oils [76]. As a result, two-phase lubricants are expected to exhibit excellent tribological performance in automotive engine systems where temperature varies with operating conditions.

Previous studies have shown the effectiveness of two-phase lubricants consisting of PAO and PAG for tribological properties. Yamada et al. found that the friction coefficient of the two-phase lubricant varies with temperature [77]. The paper reported that the two-phase lubricant maintained the same friction coefficient of 0.07 from 30 to 80 °C, while PAO showed a higher friction coefficient of more than 0.10 at all temperatures, and PAG showed a decreasing trend in friction coefficient with increasing temperature (0.12 at 30 °C and 0.011 at 80 °C). The results clearly indicated that the two-phase lubricant was effective in obtaining a constant friction coefficient with respect to temperature changes. Yamada et al. also conducted in situ observations of sliding surfaces to clarify the unique behavior of the two-phase lubricant [77]. In recent years, in situ observations have become a very effective tool for analyzing tribological behavior that occurs during sliding. For example, Raman [78–81], FT-IR [82, 83], optical reflectance [84–91], and electric resistance measurement [92, 93] have been used to understand the transition of surface conditions during

contact. In several studies, in situ reflectance spectroscopy has been used to analyze the thickness and composition of tribofilm and oil film on friction surfaces [94]. Nishimura et al. succeeded in analyzing the thickness, refractive index, and extinction coefficient of the transformed layer of diamond-like carbon coatings in situ on the order of a few nanometers [95]. Hashizume et al. revealed the thickness and composition of nanometer-order MoDTC-derived tribofilms using in situ reflectance spectroscopy measurement [96]. Okamoto et al. successfully measured the thickness of PAO oil films formed on diamond-like carbon coatings using in situ reflectance spectroscopy measurement [97]. For two-phase lubricants, Yamada et al. revealed the unique behavior of the two-phase lubricant in which PAG with hydroxyl groups selectively adsorbed on solid surfaces to form high viscosity oil layers using in situ reflectance spectroscopy measurements [77]. Final, the analysis revealed that the high viscosity oil film layers on the two solid surfaces formed a layered fluid structure, with a low viscosity oil film layer in the center sandwiched between them. In other words, the two-phase lubricant has a viscosity distribution depending on its location, which affects the oil film flow and friction behavior. Gangopadhyay et al. conducted friction tests with PAG-based engine oil under boundary and mixed lubrication conditions, followed by surface analysis using X-ray photoelectron spectroscopy. As a result, PAG-derived ether and alcohol peaks were observed, suggesting that PAG molecules were adsorbed on the solid surface due to sliding [98]. Other studies showed that the control of surface properties of solids, especially surface energy and its hydrogen-bonding term, can affect lubricant and polymer adsorption, as well as oil film thickness and tribological properties [99–101]. Here, there is a strong need to understand the influence of surface properties (i.e., surface energy) on the frictional behavior of two-phase lubricants.

The present paper demonstrates the effect of surface energy of solid surfaces on the tribological behavior of two-phase lubricants. The oil film formed between sliding surfaces is analyzed using in situ reflectance spectroscopy. Next, we analyze the viscosity distribution of the oil film, and then describe the theoretical tribological behavior of the two-phase lubricant.

2 Experiments

2.1 Specimens

Oiliness strongly depends on surface properties (i.e., surface energy of solid surface). Thus, we prepared three types of disk surfaces which have different surface energy using two types of silicone resin splay. To clarify the surface characteristics of the coated and non-coated surfaces (i.e., SUJ2 (52100 steel in the AISI standard)), we used the sessile droplet method to measure the surface energy and its hydrogen-bonding terms. A schematic of the droplet and parameters used in calculations are shown in Fig. 1. We used the half-angle method described as Eq. 1 to calculate a contact angle θ_{SL} of a droplet [102]. Pure water and diiodomethane were dropped onto the disks and width x and height y of the droplet were measured.

$$\theta_{SL} = 2\tan^{-1}\left(\frac{2y}{x}\right) \tag{1}$$

By associating Young's equation Eq. 2 and Owen's equation Eq. 3 [103], which is derived from the relation $\gamma_i = \gamma_i^d + \gamma_i^h$, Eq. 4 was derived.

$$\gamma_L \cos\theta_{SL} = \gamma_S - \gamma_{SL} \tag{2}$$

$$\gamma_{SL} = \gamma_S + \gamma_L - 2\sqrt{\gamma_S{}^d\gamma_L{}^d} - 2\sqrt{\gamma_S{}^h\gamma_L{}^h} \tag{3}$$

$$\cos\theta_{SL} = \frac{2}{\gamma_L}\sqrt{\gamma_S^d\gamma_L^d} + \frac{2}{\gamma_L}\sqrt{\gamma_S^h\gamma_L^h} - 1, \tag{4}$$

where γ_S is the solid surface tension, γ_L is the liquid surface tension, γ_{SL} is the solid/liquid interfacial surface tension. The superscript of d and h indicates the dispersion force term and hydrogen-bonding term, respectively. The γ_L, $\gamma_L{}^d$, $\gamma_L{}^h$, and θ_{SL} of water and diiodomethane were substituted into Eq. 4, and then surface energy and its hydrogen-bonding term of disks were calculated (Fig. 2). The values of water and diiodomethane used in the calculation are shown in Table 1. Figure 2 shows that the surface energy decreases after coating. The dispersion force term, value decreases from 32 to 29 mJ/m^2, resulting in 11% reduction. Furthermore, the hydrogen-bonding force term decreases from 4.6 to 0.36 mJ/m^2, resulting in 92% reduction. The reduction in

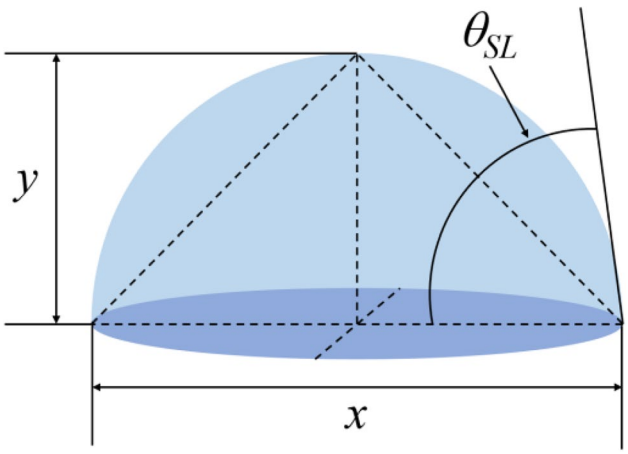

Fig. 1 A schematic of a droplet and parameters

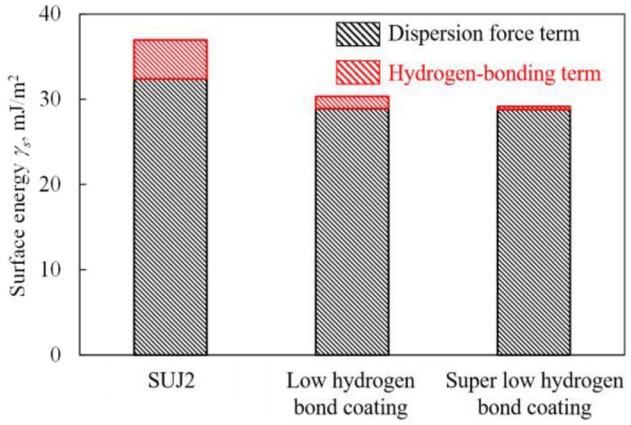

Fig. 2 Surface energy and hydrogen-bonding term of three types of disk specimens

Table 1 Properties of water and diiodomethane

	γ_L, mJ/m^2	γ_L^d, mJ/m^2	γ_L^h, mJ/m^2
Water	71.5	29.1	42.4
Diiodomethane	46.8	46.8	0

the surface energy of hydrogen-bonding term was found to be significantly higher compared to the reduction in the dispersion force term. Consequently, the total reduction in surface energy was found to be 15%. Root mean square roughness of these disk specimens were 10–12 nm, and there was no change in surface roughness before and after spraying.

Sapphire hemispheres were used as the mating material in friction tests. The hardness and Young's modulus of the sapphire hemisphere were 22.5 GPa and 470 GPa, respectively. The root mean square roughness of the sapphire hemisphere was 5.0 nm. The transmittance of the sapphire hemisphere for visible light is more than 85%. Therefore, sapphire is an excellent material for in situ measurement of reflectance in the contact area.

2.2 Pin-on-Disk Friction Test with In Situ Reflectance Spectroscopy

Figure 3 shows a schematic of the pin-on-disk type friction tester with reflectance spectroscopy. The friction tester used a sapphire hemisphere as the mating material, and the reflectance spectroscopy was located vertically above the hemisphere. Therefore, the device allowed in situ measurement of a sliding point. The reflectance spectroscopy measured the reflectance spectrum at the friction contact area through the sapphire hemisphere. The measurement-spot diameter was 10 µm, which was smaller than Hertz's contact diameter of 18 µm. The friction tests were conducted at a normal load of 0.3 N, a mean contact pressure of 300 MPa, a test

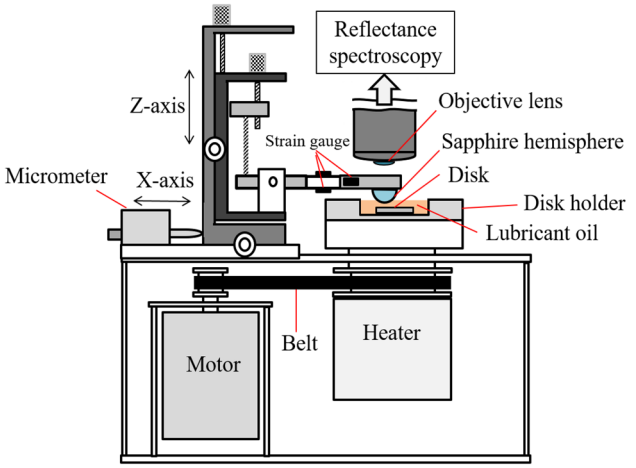

Fig. 3 A schematic of the ball-on-disk friction tester with a reflectance spectroscopy

Table 2 Friction test conditions

Three types of disk *vs.* Sapphire hemisphere	
Lubricants	Two-phase lubricant (mineral oil and colored PAG)
Normal load	0.3 N
Temperature	50 °C
Sliding speed	15.6 mm/s
Mean Hertzian contact pressure	300 MPa
Test duration	30 min

temperature of 50 °C, a sliding speed of 15.6 mm/s, and a test duration of 30 min (Table 2).

We used a two-phase lubricant which consisted of mineral oil and colored PAG (polyalkylene gycol). The colored PAG increased the gap of refractive index between the mineral oil and colored PAG to 0.05. In the reflectance spectroscopy system, the minimum resolution of refractive index was 0.01. Hence, the enlarged gap improved the accuracy of analysis in optical properties. In the present study, the oil film thickness is described with an accuracy with 1 nm. The reflectance microscopy is commonly used in semiconductor manufacturing to obtain accurate film thickness for each coating. The accuracy of the device's film thickness analysis is said to be less than 1 nm. Furthermore, several studies using the same equipment have shown that accurate film thickness can be measured with an error of 0.1–0.2 nm compared to mechanical observation methods [91, 104]. The viscosity of mineral oil and colored PAG at 50 °C under atmospheric pressure were 12.7 and 143 mPa•s, respectively. The preparation method of two-phase lubricant was the same as that of Yamada et al. [77]. Mineral oil and colored PAG were poured into a beaker at a

volumetric ratio of 1:1 at 50 °C. The lubricants were stirred thoroughly and then allowed to stand still for 30 min. The top surface of the lubricant in the beaker was used as a two-phase lubricant for the friction test. The test lubricant on the upper surface contained 30 vol% colored PAG.

2.3 Reflectance Fitting

Using post-analysis software (OPTM, Otsuka Electronics Co., Ltd., Japan), the thickness of the oil film and the composition of the two-phase lubricant at the contact position were calculated by adjusting parameters to fit an estimation curve to an obtained reflectance spectrum. The reflectance spectrums were calculated using Eq. 5.

$$R = \frac{\mathrm{Intensity\,of\,reflected\,light}}{\mathrm{Intensity\,of\,incident\,light}} \tag{5}$$

Figure 4 shows the optical model of the friction area lubricated with the two-phase lubricant. In the model, the upper part and substrate were sapphire and SUJ2, respectively. The analytical layer consisted of three lubricant layers. In the previous study, Yamada et al. revealed that the lubricant phase with highly polar function groups is attracted to the solid surfaces due to thermodynamic stability [77]. In the present model, we simulated the thin layer, where strongly attracted lubricant mainly existed, by dividing the lubricant layer into three layers. The theoretical reflectance spectrums of the optical model $R_{01234567}$ were calculated by Eqs. 6–15 [105]. The subscripts 0–7 indicate the number of layers.

$$R_{01234567} = \left|r_{01234567}\right|^2 \tag{6}$$

$$r_{01234567} = \frac{r_{01} + r_{1234567}\exp\left(-i2\beta_1\right)}{1 + r_{01}r_{1234567}\exp\left(-i2\beta_1\right)} \tag{7}$$

$$r_{1234567} = \frac{r_{12} + r_{234567}\exp\left(-i2\beta_2\right)}{1 + r_{12}r_{234567}\exp\left(-i2\beta_2\right)} \tag{8}$$

$$r_{234567} = \frac{r_{23} + r_{34567}\exp\left(-i2\beta_3\right)}{1 + r_{23}r_{34567}\exp\left(-i2\beta_3\right)} \tag{9}$$

$$r_{34567} = \frac{r_{34} + r_{4567}\exp\left(-i2\beta_4\right)}{1 + r_{34}r_{4567}\exp\left(-i2\beta_4\right)} \tag{10}$$

$$r_{4567} = \frac{r_{45} + r_{567}\exp\left(-i2\beta_5\right)}{1 + r_{45}r_{567}\exp\left(-i2\beta_5\right)} \tag{11}$$

$$r_{567} = \frac{r_{56} + r_{67}\exp\left(-i2\beta_6\right)}{1 + r_{56}r_{67}\exp\left(-i2\beta_6\right)} \tag{12}$$

$$N_m = n_m - ik_m (m = 0, 1, 2, 3, 4, 5, 6, 7 N_m, n_m \mathrm{and} k_m \mathrm{dependon wavelength} \lambda) \tag{13}$$

$$r_{ij} = \frac{N_i\cos\theta_i - N_j\cos\theta_j}{N_i\cos\theta_i + N_j\cos\theta_j} (i = 0, 1, 2, 3, 4, 5, 6 j = i + 1) \tag{14}$$

$$\beta_m = \frac{2\pi t_m N_m \cos\theta_m}{\lambda}, \tag{15}$$

where N_m is complex refractive index, which is determined by refractive index n and extinction coefficient k, and r_{ij} is amplitude reflection coefficient. The theoretical reflectance

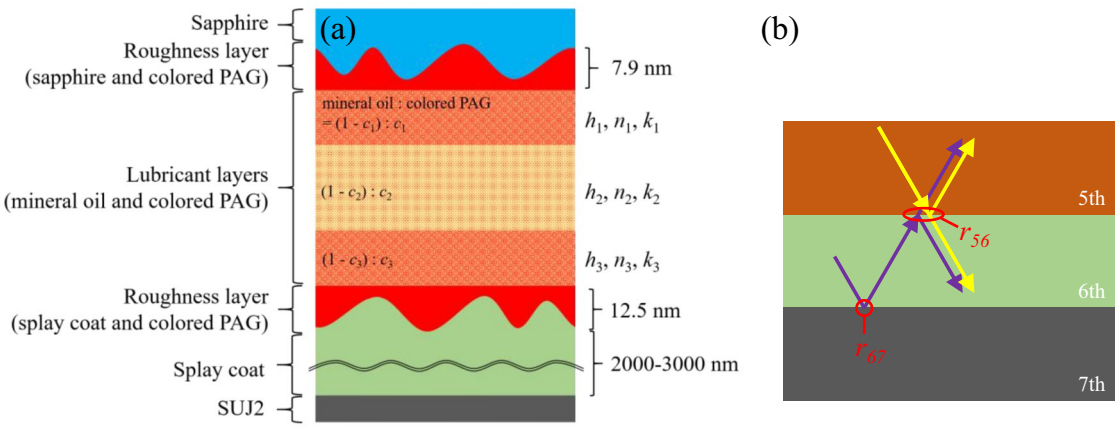

Fig. 4 **a** Optical model of the friction area lubricated with two-phase lubricant, and **b** diagram showing the relation between reflected light and r_{ij} parameters

spectrums $R_{01234567}$, which includes the results of reflection in the lower layers, were fitted to the experimentally measured reflectance spectrum (e.g., Fig. 7 showed in the section that follows) using the nonlinear least-squares method to obtain the thickness h_1, h_2, h_3, refractive index n_1, n_2, n_3, and extinction coefficient k_1, k_2, k_3. The refractive index n_1, n_2, n_3 and extinction coefficient k_1, k_2, k_3 were used to calculate the volumetric concentration of mineral oil and colored PAG in each lubricant layer. To calculate the volumetric concentration, we used the theory of effective medium approximation shown in Eqs. 16 and 17.

$$c_k \frac{\varepsilon_{mineral\,oil} - \varepsilon_k}{\varepsilon_{mineral\,oil} + 2\varepsilon_k} + \left(1 - c_k\right) \frac{\varepsilon_{colored\,PAG} - \varepsilon_k}{\varepsilon_{colored\,PAG} + 2\varepsilon_k} = 0 (k = 1, 2, 3) \tag{16}$$

$$\varepsilon = N^2 = \left(n^2 - k^2\right) - i(2nk), \tag{17}$$

where ε is dielectric constant, which can be calculated as the square of the complex refractive index.

Here, a concrete explanation of the parameters will be briefly explained using Fig. 4. In the present study, the 0th layer corresponds to sapphire and the 7th layer corresponds to the SUJ2 substrate. The reflection between the 6th and 7th layers can be calculated using Eq. 14. Subsequently, when considering the reflectance of 6th layer (between the 5th layer and 6th layer), we need to consider not only the reflectance of the boundary but also the reflected light from 7th layer (Fig. 4b). Therefore, Eq. 12 shows that r_{567} also includes the term r_{67}. Continuing this same calculation, Eqs. 6 and 7 are eventually derived, which are expressed with variables with linked subscripts.

3 Results

3.1 The Effect of Surface Energy of Sliding Surfaces on Friction Behavior of Two-Phase Lubricant

Figure 5 shows friction evolutions of the three different surface energy specimens in two-phase lubricant. These three specimens with different surface energy characteristics show unique behaviors; the lowest friction coefficient of 0.035 was observed with the SUJ2 disk from 20 to 30 min; the low hydrogen-bonding coating showed a friction coefficient of 0.044, which was the second lowest value; the superlow hydrogen bond coating showed comparably high friction coefficient of 0.050. These friction tests were conducted three times each, and similar friction coefficients were obtained in all cases. The results clearly indicate that the higher surface energy, the lower the friction coefficient. Surface energy is generated from the unbalanced surface tension

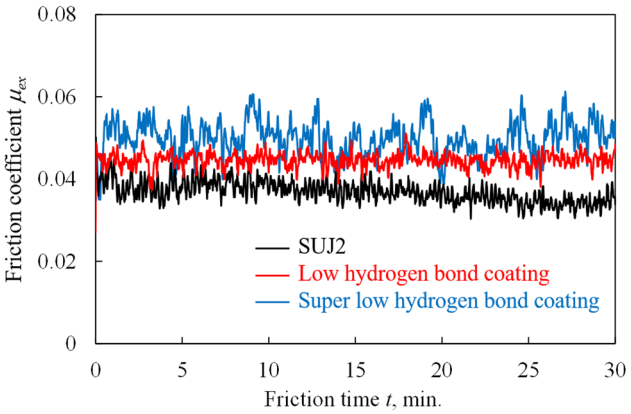

Fig. 5 Friction curves in two-phase lubricant with different surface energy specimens

due to surface where no opposing substance exists. In general, high-surface energy condition is a state in which excess energy attracts other molecules, resulting in higher oiliness. The improved oiliness may develop a moderately thicker oil film. The resulting higher surface energy decreasing the fluctuation of the friction coefficient provides evidence to support this mechanism.

After the friction tests, the surfaces of the three types of disks were observed using an optical microscope (BX60M, Olympus Corporation, Japan). The images are shown in Fig. 6a–c. No wear track with a Hertzian contact diameter of 36 µm was observed on any of the disk surfaces. From the point of view of the Stribeck curve, a hydrodynamic lubrication condition with sufficient film thickness preventing solid/solid contact should result in negligible wear. The result that no wear track was observed in the present friction tests indicates a hydrodynamic lubrication condition. The single oil film thickness calculations provided a new perspective. Lubrication conditions were calculated for pure mineral oil and pure colored PAG, respectively. Here, we used Dowson's formula [106] for the calculation. As a result, the pure mineral oil case showed boundary lubrication with an oil film thickness ratio, which presents the ratio of calculated oil film thickness to composite surface roughness, of 1.6 (calculated oil film thickness was 17 nm) and the pure colored PAG case showed hydrodynamic lubrication with an oil film thickness ratio of 8.1 (calculated oil film thickness was 91 nm). Due to two-phase lubricant is a mixture of the mineral oil and colored PAG, the lubrication condition can be considered as an intermediate one.

3.2 In Situ Measurement of Oil Film Thickness and its Composition Using a Reflectance Microscopy

To clarify the lubrication mechanism of a two-phase lubricant, we conducted in situ measurement of oil film thickness

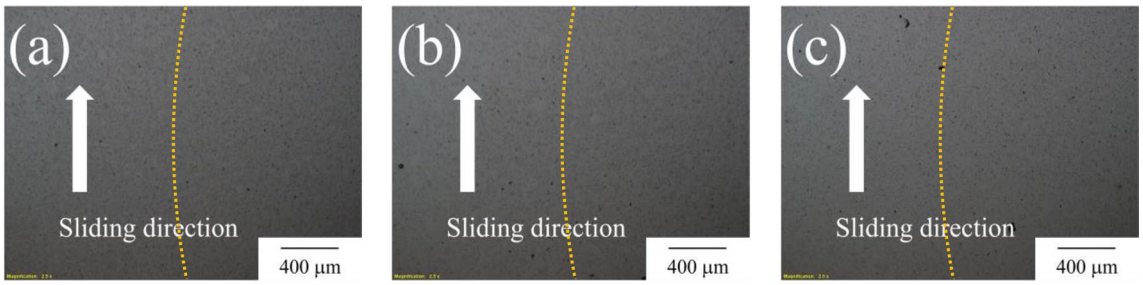

Fig. 6 Optical images of **a** SUJ2, **b** low hydrogen bond coating, and **c** superlow hydrogen bond coating after friction test (Hertzian contact diameter during the test was 36 μm). Yellow dot lines indicate the center of the wear track

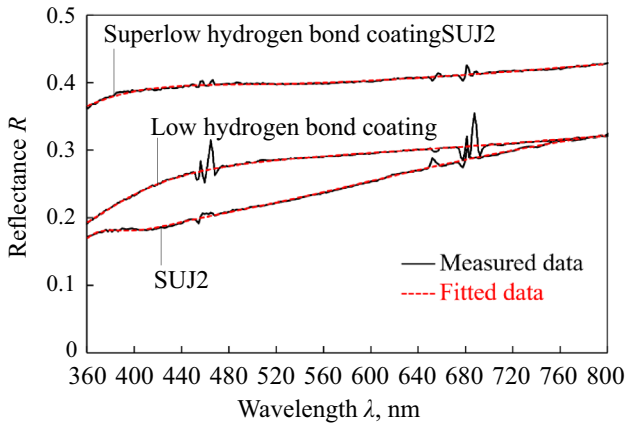

Fig. 7 Measured reflectance spectrums (black lines) and fitted reflectance spectrums (red lines) on SUJ2, low hydrogen bond coating, and superlow hydrogen bond coating

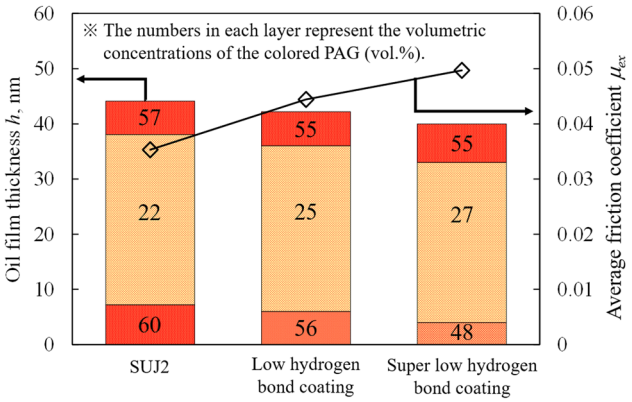

Fig. 8 Analysis result of oil films of the two-phase lubricant and experimental friction coefficients. An oil film thickness of each layer and its composition is described. Numbers described in the bar graph indicate volumetric concentration of colored PAG in layers

and its composition using a reflectance microscopy. Reflectance spectra at friction points were measured during the friction tests. Subsequently, we analyzed the oil film thickness and its composition. First, to confirm the optical properties and a thickness of each layer, parameter fitting was conducted as a shape of an estimated spectrum curve fit to the measured spectrum curve. Figure 7a–c shows the measured and fitted reflectance spectrums.

Figure 8 shows the results of oil film analysis of a two-phase lubricant and the experiment friction coefficients. First, the larger the surface energy of the hydrogen-bonding term, the larger the total oil film thickness; a total oil film thickness of 44 nm was formed on the SUJ2 specimen; a total film thickness of 42 nm was formed on low hydrogen bond coating, and a total oil film thickness of 40 nm was formed on superlow hydrogen bond coating. The lambda values, which present the ratio of calculated oil film thickness to composite surface roughness, ranged 3 to 4, indicating hydrodynamic lubrication conditions. Second, the thickness of the layer on the metal surface varies; the thickest layer thickness of 7 nm was on the SUJ2; the low hydrogen bond coating showed a thickness of 6 nm, which was the second thickest value; the superlow hydrogen bond coating showed the thinnest value of 4 nm. Third, the specimens showed different volumetric concentrations of colored PAG at the bottom layers; the SUJ2 disk showed the highest concentration of 60 vol%; the low hydrogen bond coating showed concentration of 56 vol%, which was the second highest value; the superlow hydrogen bond coating showed the lowest concentration of 48 vol%. Furthermore, the specimens also show different volumetric concentrations of colored PAG at intermediate layers; the SUJ2 disk showed the lowest concentration of 22 vol%; the low hydrogen bond coating showed concentration of 25 vol%, which was the second lowest value; the superlow hydrogen bond coating showed the highest concentration of 27 vol%. Consequently, these results show that the higher the surface energy of solid surface, the thicker the oil film thickness and the higher PAG concentration.

Described above, the three specimens were different in thickness of layers and volumetric concentration of colored PAG, causing variation of viscosity of the oil. Here, we calculated viscosity of each layer using Eq. 18.

$$\eta_k = c_k \eta_{colored\ PAG} + (1 - c_k)\eta_{mineral\ oil} \tag{18}$$

Figure 9 shows the calculated viscosities of each layer. Here, interestingly, when the bottom layer has higher viscosity, the viscosity of the intermediate layer shows lower value, and vice versa. This is due to the PAG concentration of each layer (compare the PAG concentration value in Fig. 8 and viscosity in Fig. 9). The viscosity distribution should have an important effect on the friction. Generally, both high viscosity and low viscosity characteristics are important in lubrication; the high viscosity prevent severe solid contact at low sliding speed and high normal load; the low viscosity decreases hydrodynamic resistance in hydrodynamic lubrication condition. When the two-phase lubricant provides distribution of PAG concentration and viscosity, the lubrication system can develop a thick oil film due to a high viscosity layer and low friction due to a low shear layer.

Here, we check a mean volumetric concentration of colored PAG in the entire oil film at the contact point using Eq. 19.

$$c_{mean} = \frac{c_1 h_1 + c_2 h_2 + c_3 h_3}{h_1 + h_2 + h_3} \tag{19}$$

As a result, the volumetric concentrations of the entire oil films were almost a same value of 33–34 vol% (Fig. 10), which was almost the same value as the volumetric concentration of 30 vol% for the test oil. This reveals that the global concentration of colored PAG flowing into the contact position does not change even if specimens with different surface energy are used. On the other hand, we clearly see that the surface energy affects the friction (Figs. 5 and 8). Consequently, it is indicated that the viscosity distribution due to PAG concentration causes the difference in the friction behavior.

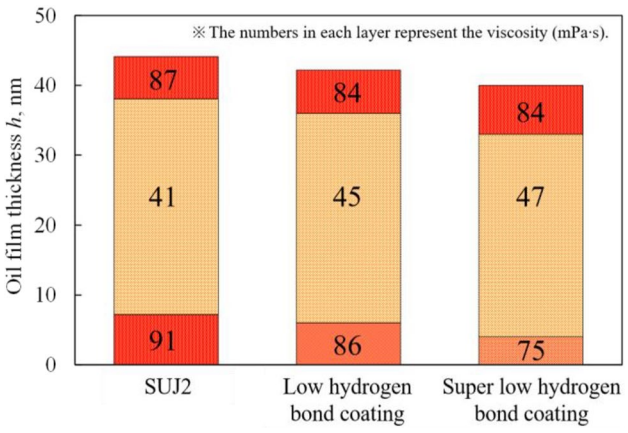

Fig. 9 Calculated viscosity of each layer

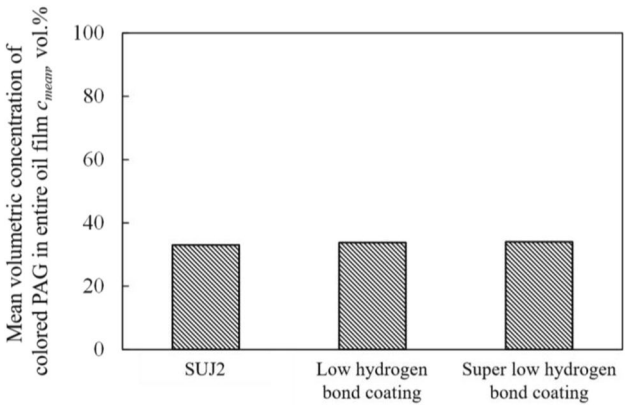

Fig. 10 Mean volumetric concentration of colored PAG in entire oil film

4 Discussions

4.1 The Effect of Surface Energy on Oil Film Composition of Two-Phase Lubricant

The yellow line in Fig. 11 shows the relationship between the hydrogen-bonding term in the surface energy of the three specimens and the volumetric concentration of colored PAG in the bottom layer (metal surface side). The SUJ2 specimen with the largest hydrogen-bonding term of 4.6 mJ/m^2 had the largest PAG volumetric concentration of 60 vol%. The specimen with the second largest hydrogen-bonding term of 1.4 mJ/m^2 had the second largest volumetric concentration of 56 vol%. The specimen with the smallest hydrogen-bonding term of 0.36 mJ/m^2 had the smallest volumetric concentration of 48 vol%. The red line in Fig. 11 indicates the relationship between the hydrogen-bonding term in the surface energy and the

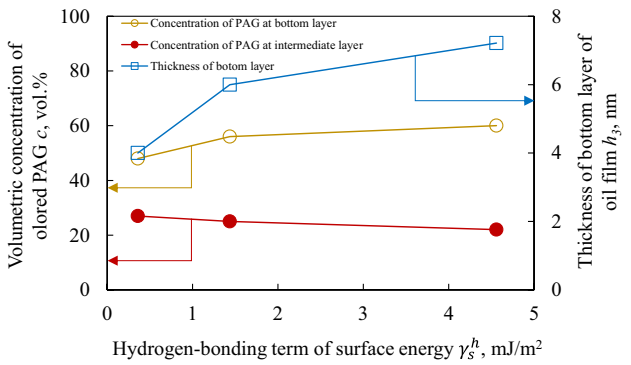

Fig. 11 Relation between hydrogen-bonding term of surface energy and the volumetric concentration of colored PAG in the bottom layer, the concentration in the intermediate layer, and the thickness of the bottom layer

volumetric concentration of colored PAG in the intermediate layer of two-phase lubricant oil film. The trend of the volumetric concentration in the intermediate layer of the oil film was opposite to that in the bottom layer. The specimen with the largest hydrogen-bonding term of 4.6 mJ/m^2 had the smallest volumetric concentration of 22 vol%. The specimen with the second largest hydrogen-bonding term of 1.4 mJ/m^2 had the second smallest volumetric concentration of 25 vol%. The specimen with the smallest hydrogen-bonding term of 0.36 mJ/m^2 had the largest volumetric concentration of 27 vol%. The blue line in Fig. 11 shows the relationship between the hydrogen-bonding term in the surface energy and the thickness of the bottom layer. The specimen with the largest hydrogen-bonding term of 4.6 mJ/m^2 had the thickest bottom layer of 7 nm. The specimen with the second largest hydrogen-bonding term of 1.4 mJ/m^2 had the second thickest bottom layer of 6 nm. The specimen with the smallest hydrogen-bonding term of 0.36 mJ/m^2 had the thinnest bottom layer of 4 nm. The trends can be summarized as follows. A larger hydrogen-bonding term of surface energy provides a larger volumetric concentration of colored PAG in the bottom layer, a smaller volumetric concentration of colored PAG in the intermediate layer, and a thicker oil film of the bottom layer. PAG contains polar functional groups (i.e., hydroxyl group) whereas mineral oil is the completely straight hydrogen carbon without function groups. Therefore, the PAG molecules are strongly attracted and adsorbed onto the surfaces with high hydrogen-bonding term of surface energy, resulting in the high viscosity of the bottom layer (metal side). This leads to a decrease in the volumetric concentration of colored PAG in the intermediate layer, leading to a lower viscosity.

4.2 The Effect of Oil Film Composition of Two-Phase Lubricant on Friction

Figure 8 clearly summarizes the relationship between the friction coefficient, oil film thickness, and the volumetric concentration of PAG in the two-phase lubricant. Whereas all tests were conducted under hydrodynamic lubrication conditions and used same two-phase lubricant, the friction coefficient varied depending on surface energy. The SUJ2 specimen showing the lowest friction coefficient had the highest volumetric concentration of colored PAG in the bottom layer, while the intermediate layer was thicker and has less volumetric concentration of colored PAG. Surface characteristics (i.e., surface energy and electrical charge) strongly affects wettability, adhesion, and adsorption characteristics [107–112]. It has been known that the molecules with polar structure (e.g., carboxy group and carbonyl group) adsorb well on solid surfaces [113–115]. In the present case, the PAG contains oxygen atoms, resulting in polar characteristics. The facts may indicate that the intermediate layer with low viscosity and low shear resistance is mainly sheared, while high viscosity layers on the surfaces supports the increase in film thickness. Therefore, we try to clarify the unique phenomenon of two-phase lubricant by estimating the friction coefficient using a hydrodynamic theory.

In the present study, we assume that the lubricants are Newtonian fluids and Couette flow is occurring because the oil film thickness is very small (on the order of nanometers) [116, 117]. Figure 12 shows Couette flow of lubricants whose viscosity is distributed in a layered structure like the two-phase lubricant. The parameters used to formulate the theoretical friction coefficient are also shown in Fig. 12. Equation 20 is derived from the relationship between velocity gradient and slip velocity.

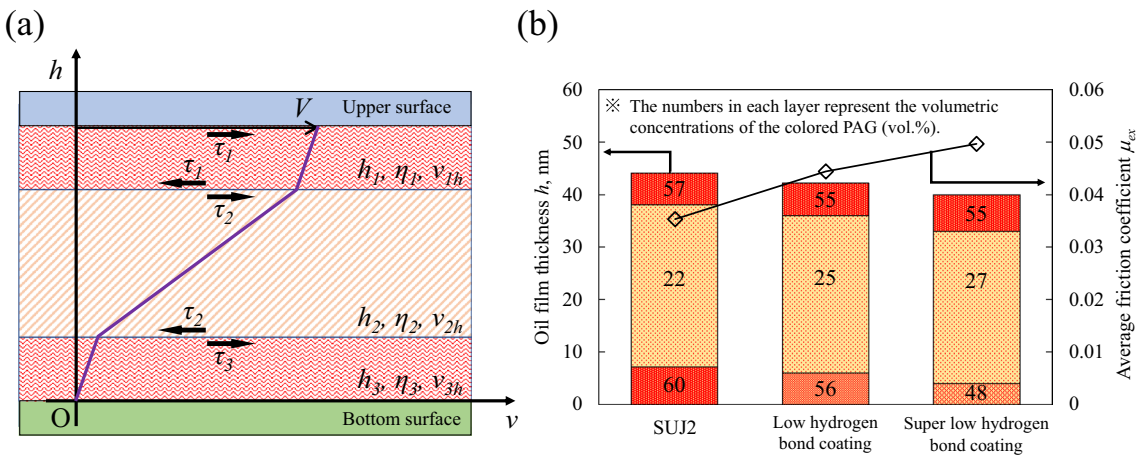

Fig. 12 **a** A schematic of Couette flow of lubricants whose viscosity is distributed in a layered structure. The purple line indicates the distribution of the velocity. **b** Re-emergence figure from Fig. 8 to better understand the model shown in (**a**) and to improve the readability of the discussion section

$$h_1 v_{1h} + h_2 v_{2h} + h_3 v_{3h} = V \tag{20}$$

Equation 21 is derived from the continuity of the shear stress at the interface of each layer.

$$\tau_1 = \tau_2 = \tau_3 \tag{21}$$

Applying the Newton's viscosity law to Eq. 21, Eq. 22 is derived.

$$\eta_1 v_{1h} = \eta_2 v_{2h} = \eta_3 v_{3h} \tag{22}$$

The conjunction of Eq. 20 and Eq. 22 leads to Eq. 23.

$$\tau_1 = \frac{V}{\sum_{k=1}^{3} \left(\frac{h_k}{\eta_k} \right)} \tag{23}$$

We assume that the viscosity of each layer is determined from the viscosity of the mineral oil and colored PAG and their volumetric concentration. Therefore, we applied Eq. 18 to Eq. 23, and then Eq. 24 is derived.

$$\tau_1 = \frac{V}{\sum_{k=1}^{3} \left[\frac{h_k}{c_k \eta_{mineral\,oil} + (1-c_k)\eta_{colored\,PAG}} \right]} \tag{24}$$

η is the viscosity of the lubricants at atmospheric pressure, but the friction surface is subjected to a mean Hertzian pressure of 294 MPa, causing an increase in a viscosity of oil. Therefore, the viscosity of the oil film is modified using Eq. 25 from the viscosity-pressure coefficient α of mineral oil and the Barus's law [118].

$$\tau_1 = \frac{V}{\sum_{k=1}^{3} \left[\frac{h_k}{c_k \eta_{mineral\,oil} + (1-c_k)\eta_{colored\,PAG}} \right] \bullet \frac{1}{\exp(\alpha p_{mean})}} \tag{25}$$

The viscosity of the lubricant increases at the Hertzian contact area. Hence, assuming that the shear force at the Hertzian contact area is dominant in the friction coefficient, the friction coefficient can be calculated as Eq. 26.

$$\mu_{th} = \frac{V}{\sum_{k=1}^{3} \left[\frac{h_k}{c_k \eta_{mineral\,oil} + (1-c_k)\eta_{colored\,PAG}} \right] \bullet \frac{1}{\exp(\alpha p_{mean})}} \bullet \frac{A}{W} \tag{26}$$

We applied the results of oil film analysis in Fig. 11 to Eq. 26. Theoretical and experimental friction coefficients are compared in Fig. 13. The correlation coefficient is 0.98, indicating that Eq. 26 is able to calculate the friction coefficient with good accuracy.

To consider the effect of the viscosity distribution of two-phase lubricant oil film on the friction coefficient, we calculated the change in the theoretical friction coefficient calculated from Eq. 26. The result is shown in Fig. 14a. In this calculation, c_3 and h_3 were the independent variables. Also, because of the results in Fig. 10c2 was the dependent variable constrained by Eq. 27.

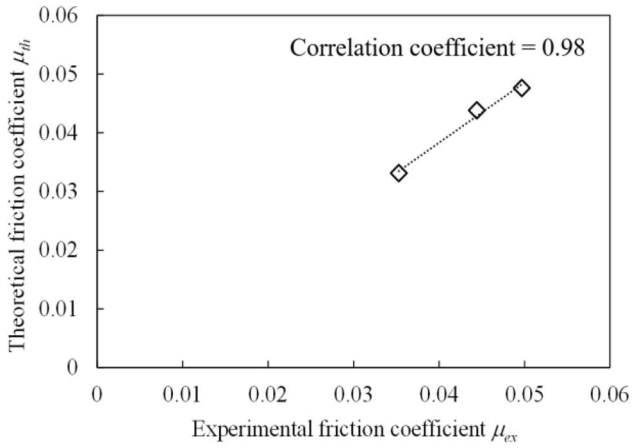

Fig. 13 Friction coefficient of friction tests and theoretical calculation

$$c_{mean} = \frac{c_1 h_1 + c_2 h_2 + c_3 h_3}{h_1 + h_2 + h_3} = 0.34 \tag{27}$$

Figure 14b shows the analytical results for c_2.

From Fig. 14a, the guideline for reducing the friction coefficient in two-phase flow is clear; the friction coefficient decreases as the oil film thickens, and the coefficient decreases whether the volume concentration of colored PAG in the bottom layer c_3 is high or low. In the present study, the mineral oil (low viscosity and non-polar) and colored PAG (high viscosity and high-polarity) were used as lubricants. As shown in Fig. 8, colored PAG tends to adsorb on the solid surface rather than concentrate in the intermediate oil film, indicating a higher concentration ratio of PAG in the bottom layer. Therefore, it is reasonable to assume that c_3 is generally 50 vol% or higher. Therefore, the general design strategy for low friction two-phase lubricants is to achieve systems that exhibit both high h_3 and c_3. Figure 14b shows the tendency for the volume concentration of colored PAG in the intermediate layer c_2 to vary with h_3 and c_3: c_2 decreases as h_3 and c_3 increase in the range where c_3 exceeds 50 vol%. This trend is easily understood as the amount of PAG in the intermediate layer decreases when PAG concentrates in the bottom layer or when the thickness of such PAG-rich oil film increases. When c_2 is low, the viscosity of the intermediate layer is small. And conversely, the viscosity of the bottom layer of the oil film is large. As a result, the shear force in the intermediate layer becomes smaller and the layer is easily sheared. This is thought to lead to a reduction in the friction coefficient. Here, it can be said that a two-phase lubricant naturally undergoes an ideal change in which the viscosity of the intermediate layer becomes smaller as the thickness and viscosity of the bottom layer increase. Here, it is worth noting again that the result is obtained with several assumptions. Several previous studies have shown that when two oils with different dielectric constants are mixed, multiple oil

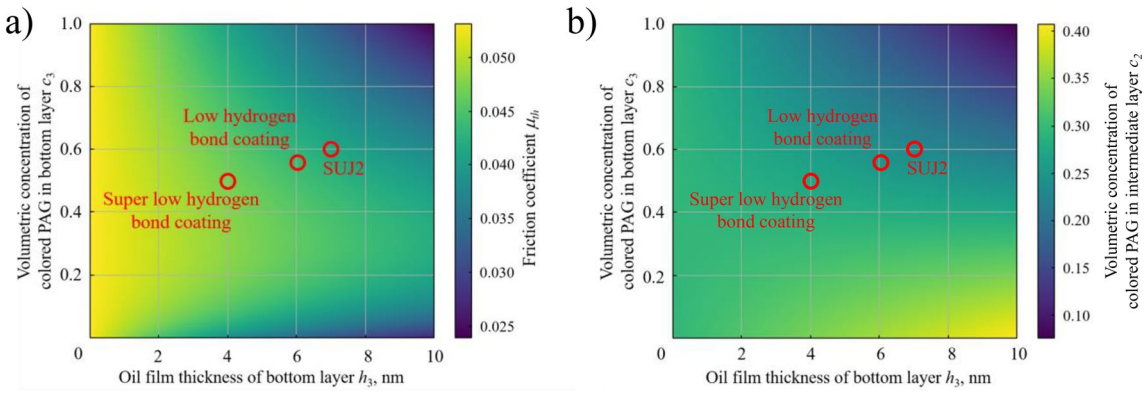

Fig. 14 Mappings of **a** the theoretically calculated friction coefficient and **b** the volumetric concentration of colored PAG in the intermediate layer. Red circles are tested conditions shown in Fig. 13

layers are formed due to the formation of an adsorption layer of the oil with the higher dielectric constant [77, 119]. In the present study, two different models (i.e., one homogeneous oil film and a multilayer oil film) were compared, and the multilayer model showed higher fitting accuracy. Therefore, the multilayer model is appropriate for the sliding conditions in the present study as in previous studies. On the other hand, there should be some limitations to the assumptions, such as pressure, sliding velocity, balance between surface and liquid surface free energy, and severity of boundary lubrication conditions. In addition, changes in some friction conditions (e.g., very high pressure or very high shear rate) will also alter the behavior of the fluid. Therefore, it must be remembered that the friction estimation, especially Fig. 14, is applicable when the conditions are maintained.

In order to achieve such low friction conditions, the control of surface energy plays an important role. Generally, in two-phase lubricants, the oil with higher viscosity has higher polarity. Therefore, a surface with a large hydrogen-bonding term in the surface energy should attract high viscosity oil molecules and form a thick high viscosity oil film layer on the solid surface. As a result, sufficient load-carrying capacity can be achieved. In addition, as mentioned above, the attraction of high viscosity oil to the surface reduces the concentration of the high viscosity oil in the intermediate layer. As a result, the shear force is reduced, allowing it to carry a larger velocity gradient, and the friction coefficient decreases as a response of the lubrication system (Fig. 15).

Considering actual automobile engine systems, the temperature varies with operating conditions. In the present study, we clarify the unique behavior of the two-phase lubricant at low temperatures, where complete mixing of low viscosity and high viscosity lubricants does not occur. As a result, a new behavior was found in which high-polar high viscosity oil tends to adsorb on solid surfaces, while low viscosity oil concentrates between the layers of high viscosity oil film. As temperature increases, the solubility of the two oils increases. On the other hand, previous studies on two-phase lubricants showed that even at 80 °C conditions in nanoscale gaps, there is a separation between a high viscosity phase formed on the solid surfaces and a low viscosity phase sandwiched between the two [77]. Therefore, although it remains an interesting subject for future studies, the new findings on the effect of surface energy on tribological behavior described in the present paper can be applicable to varying temperature conditions.

In actual machine parts, the effect of additives in oil lubricants is very important. In the present paper, oil lubricants

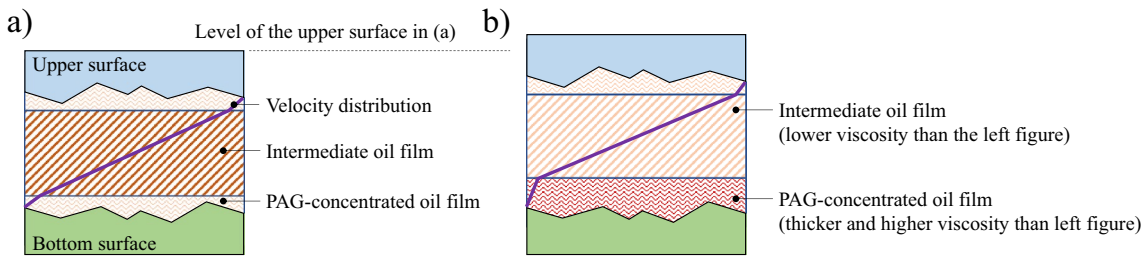

Fig. 15 Schematics of the difference in the velocity distribution for **a** the low hydrogen bond surface and **b** the high hydrogen bond surface

without additives are used. Therefore, a clear trend of the two-phase lubricant can be shown. Considering additives, differences in solubility of additives in the two lubricants may influence the friction behavior, especially under boundary lubrication conditions. Peeters et al. simulated the behavior of additive molecules and found that ZDDP additives tend to adsorb on the surface with higher surface free energies [120]. From this result, it can be inferred that additive molecules, which generally has several amounts of polarity, dissolve more in highly polar and high viscosity oils. As revealed in the present paper, highly polar oils tend to adsorb on solid surfaces. Therefore, two-phase lubricants are expected to exhibit excellent low friction behavior even under additive-containing conditions. The lubrication conditions in the present paper are hydrodynamic lubrication conditions. Due to the hydrodynamic lubrication condition and the non-additive-containing condition, the present paper successfully demonstrate the general trend of the two-phase lubricant, while their behavior under boundary lubrication conditions is a very interesting future study.

5 Conclusions

In the present paper, the effect of surface energy of solid surfaces on the tribological behavior of two-phase lubricants is investigated. Using a two-phase lubricant consisting of low viscosity non-polar mineral oil and high viscosity high-polar PAG, the SUJ2 specimen (showing a high hydrogen-bonding term in the surface energy components) recorded the lowest friction coefficient of 0.035, while the superlow hydrogen bond coating recorded the highest coefficient of 0.050. The reflectance spectroscopy of the friction surfaces observed in situ were analyzed to calculate the thickness of the oil film and the volume concentration distribution of the colored PAG. First, the specimens with larger hydrogen-bonding terms formed thicker oil films. Second, the thickness of the bottom layer and the concentration of PAG in the bottom layer were larger for the specimens with larger hydrogen-bonding terms. This also resulted in a lower concentration of colored PAG in the intermediate layer of the oil film. Calculation of the theoretical friction coefficient assuming Couette flow reveals important factors that reduce the friction coefficient in two-phase lubricant. Similar to the experimental results, the higher the PAG concentration in the bottom oil layer, the lower the friction coefficient. The decrease in PAG concentration in the intermediate layer also follows this change, and the shear resistance of the layer can decrease. The experimental and analytical results suggest that the normal load is supported on the high viscosity oil layers formed on the solid surfaces, while the low viscosity intermediate layer undergoes shear due to its low viscosity characteristics, resulting in low friction as a system. It should be noted here again that this result is established under certain sliding conditions where adsorbed oil layers and Newtonian fluid behavior are developed. On the other hand, the present paper, while based on these assumptions, provides a comprehensive understanding of the effect of the multilayer oil distribution on the friction coefficient. It is also clarified that surfaces with a large hydrogen-bonding term in the surface energy components play an important role in the development of this condition.

Author Contributions KH: Investigation, Writing – original draft. MM: Investigation, Project administration, Writing – original draft. NU: Conceptualization, Project administration, Resources, Supervision, Writing – review & editing. TT: Methodology, Writing – review & editing. W-YL: Methodology, Writing – review & editing. NH: Methodology, Writing – review & editing. TS: Methodology, Writing – review & editing. RN: Methodology, Writing – review & editing. KH: Methodology, Writing – review & editing. AO: Methodology, Writing – review & editing. MU: Methodology, Writing – review & editing.

Funding The authors have not disclosed any funding.

Data Availability All datasets generated or analyzed during the current study are described as presented figures or tables. The data used in this study are available upon request.

Declarations

Conflict of interest The authors declare that they have no known competing financial interests or personal relationships that could have appeared to influence the work reported in this paper.

References

1. Holmberg, K., Andersson, P., Erdemir, A.: Global energy consumption due to friction in passenger cars. Tribol. Int. **47**, 221–234 (2012). https://doi.org/10.1016/j.triboint.2011.11.022
2. Erdemir, A.: The role of hydrogen in tribological properties of diamond-like carbon films. Surf. Coat. Technol. **146–147**, 292–297 (2001). https://doi.org/10.1016/S0257-8972(01)01417-7
3. Erdemir, A.: Genesis of superlow friction and wear in diamond-like carbon films. Tribol. Int. **37**, 1005–1012 (2004). https://doi.org/10.1016/j.triboint.2004.07.018
4. Liu, X., Yamaguchi, R., Umehara, N., Deng, X., Kousaka, H., Murashima, M.: Clarification of high wear resistance mechanism of ta-CNx coating under poly alpha-olefin (PAO) lubrication.

Tribol. Int. **105**, 193–200 (2017). https://doi.org/10.1016/j.triboint.2016.10.016
5. Liu, X., Yamaguchi, R., Umehara, N., Murashima, M., Tokoroyama, T.: Effect of oil temperature and counterpart material on the wear mechanism of ta-CNx coating under base oil lubrication. Wear **390–391**, 312–321 (2017). https://doi.org/10.1016/j.wear.2017.08.012
6. Sheeja, D., Tay, B.K., Lau, S.P., Shi, X., Ding, X.: Structural and tribological characterization of multilayer ta-C films prepared by filtered cathodic vacuum arc with substrate pulse biasing. Surf. Coat. Technol. **132**, 228–232 (2000). https://doi.org/10.1016/S0257-8972(00)00848-3
7. Mabuchi, Y., Higuchi, T., Yoshimura, D., Murashima, M., Kousaka, H., Umehara, N.: Influence of carbon black in engine oil on wear of H-free diamond-like carbon coatings. Tribol. Int. **73**, 138–147 (2014). https://doi.org/10.1016/j.triboint.2014.01.016
8. Ehrhardt, H.: New developments in the field of superhard coatings. Surf. Coat. Technol. **74–75**, 29–35 (1995). https://doi.org/10.1016/0257-8972(95)08212-3
9. Sjöström, H., Wikström, V.: Diamond-like carbon coatings in rolling contacts. Proceed. Inst. Mech. Eng. Part J: J. Eng. Tribol. **215**, 545–561 (2001). https://doi.org/10.1243/1350650011543790
10. Liu, X., Umehara, N., Tokoroyama, T., Murashima, M.: Tribological properties of ta-CNx coating sliding against steel and sapphire in unlubricated condition. Tribol. Int. **131**, 102–111 (2019). https://doi.org/10.1016/j.triboint.2018.10.022
11. Al Mahmud, K.A.H., Varman, M., Kalam, M.A., Masjuki, H.H., Mobarak, H.M., Zulkifli, N.W.M.: Tribological characteristics of amorphous hydrogenated (a-C: H) and tetrahedral (ta-C) diamond-like carbon coating at different test temperatures in the presence of commercial lubricating oil. Surf. Coat. Technol. **245**, 133–147 (2014). https://doi.org/10.1016/j.surfcoat.2014.02.052
12. Jones, A.H.S., Camino, D., Teer, D.G., Jiang, J.: Novel high wear resistant diamond-like carbon coatings deposited by magnetron sputtering of carbon targets. Proceed. Inst. Mech. Eng. Part J: J. Eng. Tribol. **212**, 301–306 (1998). https://doi.org/10.1243/1350650981542119
13. Bin, M.M.M., Umehara, N., Tokoroyama, T., Murashima, M., Shibata, A., Utsumi, Y., et al.: Effect of pillar and mesh structure of tetrahedral amorphous carbon (TA-C) coatings on the wear properties and fracture toughness of the coating. Tribol. Online **14**, 388–397 (2019). https://doi.org/10.2474/trol.14.388
14. Bin, M.M.M., Umehara, N., Tokoroyama, T., Murashima, M., Shibata, A., Utsumi, Y., et al.: Effect of mesh structure of tetrahedral amorphous carbon (ta-C) coating on friction and wear properties under base-oil lubrication condition. Tribol. Int. (2020). https://doi.org/10.1016/j.triboint.2019.01.016
15. Yamada, Y., Murashima, M., Umehara, N., Tokoroyama, T., Lee, W.Y., Takamatsu, H., et al.: Effect of fracture properties and surface morphology on wear of DLC coatings at severe contact condition. Tribol. Int. **169**, 107486 (2022). https://doi.org/10.1016/j.triboint.2022.107486
16. Robertson, J.: Diamond-like amorphous carbon. Mater. Sci. Eng. R. Rep. **37**, 129–281 (2002). https://doi.org/10.1016/s0927-796x(02)00005-0
17. Vetter, J.: 60years of DLC coatings: Historical highlights and technical review of cathodic arc processes to synthesize various DLC types, and their evolution for industrial applications. Surf. Coat. Technol. **257**, 213–240 (2014). https://doi.org/10.1016/j.surfcoat.2014.08.017
18. Murashima, M., Deng, X., Izuoka, H., Umehara, N., Kousaka, H.: Effect of oxygen on degradation of defects on ta-C coatings deposited by filtered arc deposition. Surf. Coat. Technol. **362**, 200–207 (2019). https://doi.org/10.1016/j.surfcoat.2019.01.115
19. Erdemir, A.: Friction and wear of diamond and diamond-like carbon films. Proceed. Inst. Mech. Eng. Part J: J. Eng. Tribol. **216**, 387–400 (2002). https://doi.org/10.1243/135065002762355316
20. Haque, T., Morina, A., Neville, A.: Tribological performance evaluation of a hydrogenated diamond-like carbon coating in sliding/rolling contact - Effect of lubricant additives. Proceed. Inst. Mech. Eng. Part J: J. Eng. Tribol. **225**, 393–405 (2011). https://doi.org/10.1177/1350650111402769
21. Gangopadhyay, A.K., Vassell, W.C., Tamor, M.A., Willermet, P.A.: Tribological behavior of amorphous hydrogenated carbon films on silicon. J. Tribol. **116**, 454–462 (1994). https://doi.org/10.1115/1.2928865
22. Murashima, M., Maeda, M., Xingrui, D., Umehara, N., Kousaka, H.: Development of a new diamond-like carbon surface treatment method with electric discharge for short running-in and friction reduction. Proceed. Inst. Mech. Eng. Part J: J. Eng. Tribol. (2021). https://doi.org/10.1177/13506501211013126
23. Lee, W.Y., Jang, Y.J., Tokoroyama, T., Murashima, M., Umehara, N.: Effect of defects on wear behavior in ta-C coating prepared by filtered cathodic vacuum arc deposition. Diam. Relat. Mater. **105**, 107789 (2020). https://doi.org/10.1016/j.diamond.2020.107789
24. Donnet, C., Martin, J.M., Fontaine, J., Sánchez-López, J.C., Quirós, C., Elizalde, E., et al.: The role of CN chemical bonding on the tribological behaviour of CNx coatings. Surf. Coat. Technol. **120–121**, 594–600 (1999). https://doi.org/10.1016/S0257-8972(99)00449-1
25. Wu, W., Murashima, M., Saso, T., Tokoroyama, T., Lee, W., Kousaka, H., et al.: New in situ superlow-friction method for nitrogen-containing diamond-like carbon coatings using dielectric barrier discharge treatment in ambient air. Tribol. Int. **174**, 107749 (2022). https://doi.org/10.1016/j.triboint.2022.107749
26. Kim, J.-I., Lee, W.-Y., Tokoroyama, T., Murashima, M., Umehara, N.: Friction characteristics of amorphous carbon coating against various 3d-transition metals. Tribol. Int. **174**, 107690 (2022). https://doi.org/10.1016/j.triboint.2022.107690
27. Kim, J.-I., Lee, W.-Y., Tokoroyama, T., Murashima, M., Umehara, N.: Tribo-chemical wear of various 3d-transition metals against DLC: influence of tribo-oxidation and low-shear transferred layer. Tribol. Int. **177**, 107938 (2022). https://doi.org/10.1016/j.triboint.2022.107938
28. Murashima, M., Oyama, S., Kousaka, H., Tokoroyama, T., Lee, W.-Y., Umehara, N.: New in situ low-friction technology for diamond-like carbon coatings using surface discharge treatment in ambient air. Tribol. Int. **165**, 107306 (2022). https://doi.org/10.1016/j.triboint.2021.107306
29. Lee, W.Y., Tokoroyama, T., Murashima, M., Umehara, N.: Investigating running-in behavior to understand wear behavior of ta-C coating with filtered cathodic vacuum arc deposition. J. Tribol. **23**, 38–47 (2019)
30. Nyberg, H., Tokoroyama, T., Wiklund, U., Jacobson, S.: Design of low-friction PVD coating systems with enhanced running-in performance - carbon overcoats on TaC/aC coatings. Surf. Coat. Technol. **222**, 48–54 (2013). https://doi.org/10.1016/j.surfcoat.2013.02.003
31. Tokoroyama, T., Hattori, T., Umehara, N., Kousaka, H., Manabe, K., Kishi, M., et al.: Ultra-low friction properties of carbon nitride tantalum coatings in the atmosphere. Tribol. Int. **103**, 388–393 (2016). https://doi.org/10.1016/j.triboint.2016.07.015
32. Vengudusamy, B., Mufti, R.A., Lamb, G.D., Green, J.H., Spikes, H.A.: Friction properties of DLC/DLC contacts in base oil. Tribol. Int. **44**, 922–932 (2011). https://doi.org/10.1016/j.triboint.2011.03.006
33. Kosarieh, S., Morina, A., Lainé, E., Flemming, J., Neville, A.: Tribological performance and tribochemical processes in a DLC/

steel system when lubricated in a fully formulated oil and base oil. Surf. Coat. Technol. **217**, 1–12 (2013). https://doi.org/10.1016/j.surfcoat.2012.11.065
34. Kosarieh, S., Morina, A., Lainé, E., Flemming, J., Neville, A.: The effect of MoDTC-type friction modifier on the wear performance of a hydrogenated DLC coating. Wear **302**, 890–898 (2013). https://doi.org/10.1016/j.wear.2012.12.052
35. Kano, M., Yasuda, Y., Okamoto, Y., Mabuchi, Y., Hamada, T., Ueno, T., et al.: Ultralow friction of DLC in presence of glycerol mono-oleate (GMO). Tribol. Lett. **18**, 245–251 (2005). https://doi.org/10.1007/s11249-004-2749-4
36. Ronkainen, H., Varjus, S., Holmberg, K.: Friction and wear properties in dry, water- and oil-lubricated DLC against alumina and DLC against steel contacts. Wear **222**, 120–128 (1998). https://doi.org/10.1016/S0043-1648(98)00314-7
37. Aboua, K.A.M., Umehara, N., Kousaka, H., Tokoroyama, T., Murashima, M., Mabuchi, Y., et al.: Effect of carbon diffusion on friction and wear behaviors of diamond-like carbon coating against germanium in boundary base oil lubrication. Tribol. Lett. **67**, 1–11 (2019). https://doi.org/10.1007/s11249-019-1179-2
38. Aboua, K.A.M., Umehara, N., Kousaka, H., Tokoroyama, T., Murashima, M., Mabuchi, Y., et al.: Effect of carbon diffusion on friction and wear behaviors of diamond-like carbon coating against Cr-plating in boundary base oil lubrication. Tribol. Online **13**, 290–300 (2018). https://doi.org/10.2474/trol.13.290
39. Aboua, K.A.M., Umehara, N., Kousaka, H., Tokoroyama, T., Murashima, M., Mabuchi, Y., et al.: Efect of mating material and graphitization on wear of a-CH coating in boundary base oil lubrication. Tribol. Lett. **68**, 1–8 (2020)
40. Bin, T.M.T., Umehara, N., Tokoroyama, T., Murashima, M.: The effects of oil additives and mating materials to the friction, wear and seizure characteristics of a-C : H coating. J. Tribol. **18**, 1–19 (2018)
41. Li, X., Sawaki, T., Kousaka, H., Murashima, M., Umehara, N.: Effect of mating materials on wear properties of amorphous hydrogenated carbon (a-C:H) coating and tetrahedral amorphous carbon (ta-C) coating in base oil boundary lubrication condition. J. Tribol. **15**, 1–20 (2017)
42. Bewilogua, K., Bräuer, G., Dietz, A., Gäbler, J., Goch, G., Karpuschewski, B., et al.: Surface technology for automotive engineering. CIRP Ann. Manuf. Technol. **58**, 608–627 (2009). https://doi.org/10.1016/j.cirp.2009.09.001
43. Kano, M.: Diamond-like carbon coating applied to automotive engine components. Tribol. Online **9**, 135–142 (2014). https://doi.org/10.2474/trol.9.135
44. Mabuchi, Y., Yamashita, T., Izumi, H., Sekikawa, T., Nishimura, K., Hirano, S., et al.: Examination of the axial shape of the automotive valvetrain cam for engine friction reduction. Tribol. Trans. **60**, 1088–1098 (2017). https://doi.org/10.1080/10402004.2016.1261312
45. Higuchi, T., Mabuchi, Y., Ichihara, H., Murata, T., Moronuki, M.: Development of hydrogen-free diamond-like carbon coating for piston rings. Tribol. Online **12**, 117–122 (2017). https://doi.org/10.2474/trol.12.117
46. Tung, S.C., Gao, H.: Tribological characteristics and surface interaction between piston ring coatings and a blend of energy-conserving oils and ethanol fuels. Wear **255**, 1276–1285 (2003). https://doi.org/10.1016/S0043-1648(03)00240-0
47. Barthlott, W., Neinhuis, C.: Purity of the sacred lotus, or escape from contamination in biological surfaces. Planta **202**, 1–8 (1997). https://doi.org/10.1007/s004250050096
48. Wang, X., Kato, K., Adachi, K., Aizawa, K.: Loads carrying capacity map for the surface texture design of SiC thrust bearing sliding in water. Tribol. Int. **36**, 189–197 (2003). https://doi.org/10.1016/S0301-679X(02)00145-7
49. Murashima, M., Umehara, N., Kousaka, H.: Effect of nano-texturing on adhesion of thermoplastic resin against textured steel plate. Tribol. Online **11**, 159–167 (2016). https://doi.org/10.2474/trol.11.159
50. Murashima, M., Imaizumi, Y., Kawaguchi, M., Umehara, N., Tokoroyama, T., Saito, T., et al.: Realization of a novel morphing surface using additive manufacturing and its active control in friction. J. Tribol. **143**, 051104-1–51111 (2021). https://doi.org/10.1115/1.4050269
51. Murashima, M., Yoshino, S., Kawaguchi, M., Umehara, N.: Intelligent tribological surfaces: from concept to realization using additive manufacturing. Int. J. Mech. Mater. Des. **15**, 757–766 (2019). https://doi.org/10.1007/s10999-018-9435-4
52. Erdemir, A.: Review of engineered tribological interfaces for improved boundary lubrication. Tribol. Int. **38**, 249–256 (2005). https://doi.org/10.1016/j.triboint.2004.08.008
53. Etsion, I.: Improving tribological performance of mechanical components by laser surface texturing. Tribol. Lett. **17**, 733–737 (2004). https://doi.org/10.1007/s11249-004-8081-1
54. Murashima, M., Yamada, T., Umehara, N., Tokoroyama, T., Lee, W.-Y.: Novel friction stabilization technology for surface damage conditions using machine learning. Tribol. Int. **180**, 108280 (2023). https://doi.org/10.1016/j.triboint.2023.108280
55. Haque, T., Morina, A., Neville, A., Kapadia, R., Arrowsmith, S.: Effect of oil additives on the durability of hydrogenated DLC coating under boundary lubrication conditions. Wear **266**, 147–157 (2009). https://doi.org/10.1016/j.wear.2008.06.011
56. Topolovec-Miklozic, K., Lockwood, F., Spikes, H.: Behaviour of boundary lubricating additives on DLC coatings. Wear **265**, 1893–1901 (2008). https://doi.org/10.1016/j.wear.2008.04.051
57. De Barros'Bouchet, M.I., Martin, J.M., Le-Mogne, T., Vacher, B.: Boundary lubrication mechanisms of carbon coatings by MoDTC and ZDDP additives. Tribol. Int. **38**, 257–264 (2005). https://doi.org/10.1016/j.triboint.2004.08.009
58. Bin, T.M.T., Umehara, N., Tokoroyama, T., Murashima, M.: The effect of UV irradiation to a-C: H on friction and wear properties under PAO oil lubrication including MoDTC and ZnDTP. Tribol. Online **13**, 119–130 (2018). https://doi.org/10.2474/trol.13.119
59. Equey, S., Roos, S., Mueller, U., Hauert, R., Spencer, N.D., Crockett, R.: Tribofilm formation from ZnDTP on diamond-like carbon. Wear **264**, 316–321 (2008). https://doi.org/10.1016/j.wear.2007.03.012
60. Podgornik, B., Vižintin, J.: Tribological reactions between oil additives and DLC coatings for automotive applications. Surf. Coat. Technol. **200**, 1982–1989 (2005). https://doi.org/10.1016/j.surfcoat.2005.08.014
61. Kalin, M., Vižintin, J.: A comparison of the tribological behaviour of steel/steel, steel/DLC and DLC/DLC contacts when lubricated with mineral and biodegradable oils. Wear **261**, 22–31 (2006). https://doi.org/10.1016/j.wear.2005.09.006
62. Komori, K., Umehara, N.: Friction and wear properties of tetrahedral Si-containing hydrogenated diamond-like carbon coating under lubricated condition with engine-oil containing ZnDTP and MoDTC. Tribol. Online **12**, 123–134 (2017). https://doi.org/10.2474/trol.12.123
63. Kassim, K.A.M., Tokoroyama, T., Murashima, M., Lee, W.Y., Umehara, N., Mustafa, M.M.B.: Wear acceleration of a-C: H coatings by molybdenum-derived particles: Mixing and temperature effects. Tribol. Int. **159**, 106944 (2021). https://doi.org/10.1016/j.triboint.2021.106944
64. Kassim, K.A.M., Tokoroyama, T., Murashima, M., Umehara, N.: The wear classification of MoDTC-derived particles on silicon and hydrogenated diamond-like carbon at room temperature. Tribol. Int. **147**, 106176 (2020). https://doi.org/10.1016/j.triboint.2020.106176

65. Li, X., Murashima, M., Umehara, N.: Effect of nanoparticles as lubricant additives on friction and wear behavior of tetrahedral amorphous carbon (ta-C) coating. J. Tribol. **16**, 15–29 (2018)
66. Aboua, K.A.M., Umehara, N., Kousaka, H., Tokoroyama, T., Murashima, M., Tasdemir, H.A., et al.: Effect of ZnDTP triboflim's morphology on friction behaviors of DLC coatings: tribofilm characterization by 3D scanning electron microscope observation. J. Adv. Mech. Des. Syst. Manuf. **12**, 1–12 (2018). https://doi.org/10.1299/jamdsm.2018jamdsm0129
67. Kinoshita, Y., Murashima, M., Kawachi, M., Ohno, N.: First-principles study of mechanical properties of one-dimensional carbon nanotube intramolecular junctions. Comput. Mater. Sci. **70**, 1–7 (2013). https://doi.org/10.1016/j.commatsci.2012.12.033
68. Mohiuddin, T.M.G., Lombardo, A., Nair, R.R., Bonetti, A., Savini, G., Jalil, R., et al.: Uniaxial strain in graphene by Raman spectroscopy: G peak splitting, Grüneisen parameters, and sample orientation. Phys. Rev. B Condens. Matter Mater. Phys. **79**, 1–8 (2009). https://doi.org/10.1103/PhysRevB.79.205433
69. Chan, K.T., Neaton, J.B., Cohen, M.L.: First-principles study of metal adatom adsorption on graphene. Phys. Rev. B Condens. Matter Mater. Phys. **77**, 1–12 (2008). https://doi.org/10.1103/PhysRevB.77.235430
70. Leenaerts, O., Partoens, B., Peeters, F.M.: Adsorption of H2 O, N H3, CO, N O2, and NO on graphene: a first-principles study. Phys. Rev. B Condens. Matter Mater. Phys. **77**, 1–6 (2008). https://doi.org/10.1103/PhysRevB.77.125416
71. Lobzenko, I., Shiihara, Y., Sakakibara, A., Uchiyama, Y., Umeno, Y., Todaka, Y.: Chemisorption enhancement of single carbon and oxygen atoms near the grain boundary on Fe surface: ab initio study. Appl. Surf. Sci. **493**, 1042–1047 (2019). https://doi.org/10.1016/j.apsusc.2019.06.250
72. Taylor, R.I., Morgan, N., Mainwaring, R., Davenport, T.: How much mixed/boundary friction is there in an engine — and where is it? Proceed. Inst. Mech. Eng. Part J: J. Eng. Tribol. **234**, 1563–1579 (2020). https://doi.org/10.1177/1350650119875316
73. Taylor, R.I., Coy, R.C.: Improved fuel efficiency by lubricant design: a review. Proceed. Inst. Mech. Eng. Part J: J. Eng. Tribol. **214**, 1–15 (2000). https://doi.org/10.1177/135065010021400101
74. Gangopadhyay, A.: A review of automotive engine friction reduction opportunities through technologies related to tribology. Trans. Indian Inst. Met. **70**, 527–535 (2017). https://doi.org/10.1007/s12666-016-1001-x
75. Peterson, K.B., Jackson, A.: Multi-phase lubricant, United States Patent Number 5602085 (1997)
76. Kamata, K., Kawamura, Y., Maruyama, R., Nagatomi, E., Tazaki, H.: The development to control simultaneously viscosity and separation temperature of a two phase lubricant for practical use. Tribol. Online **11**, 24–33 (2016). https://doi.org/10.2474/trol.11.24
77. Yamada, T., Umehara, N., Tokoroyama, T., Murashima, M., Sato, T., Ohara, K., et al.: In-situ analysis of two phase lubricant oil film with a reflectance spectroscopy. Trans. JSME (in Japanese) **86**, 19–00315 (2020). https://doi.org/10.1299/transjsme.19-00315
78. Okubo, H., Tadokoro, C., Sasaki, S.: In situ raman-SLIM monitoring for the formation processes of MoDTC and ZDDP tribofilms at Steel/Steel contacts under boundary lubrication. Tribol. Online **15**, 105–116 (2020). https://doi.org/10.2474/TROL.15.105
79. Cheng, C.L., Chia, C.T., Chiu, C.C., Lin, I.N.: Time-dependent in-situ Raman observation of atomic hydrogen etching on diamond-like carbon films. Diam. Relat. Mater. **11**, 262–267 (2002). https://doi.org/10.1016/S0925-9635(01)00695-1
80. Scharf, T.W., Singer, I.L.: Monitoring transfer films and friction instabilities with in situ Raman tribometry. Tribol. Lett. **14**, 3–8 (2003). https://doi.org/10.1023/A:1021942830132
81. Tokoroyama, T., Murashima, M., Umehara, N.: The surface enhanced raman scattering analysis for carbonaceous coating by using Au nano-particles. Tribol. Online **15**, 300–308 (2020). https://doi.org/10.2474/TROL.15.300
82. Sasaki, K., Inayoshi, N., Tashiro, K.: Friction-induced dynamic chemical changes of tricresyl phosphate as lubricant additive observed under boundary lubrication with 2D fast imaging FTIR-ATR spectrometer. Wear **268**, 911–916 (2010). https://doi.org/10.1016/j.wear.2009.12.017
83. Sasaki K, Inayoshi N, Tashir K (2009) In-situ observation of phase transition behavior of n-alkane molecules induced by friction motion on metal interface. In: World Tribology Congress - 2009 Proceedings. 32:828.
84. Guegan, J., Kadiric, A., Gabelli, A., Spikes, H.: The relationship between friction and film thickness in EHD point contacts in the presence of longitudinal roughness. Tribol. Lett. **64**, 1–15 (2016). https://doi.org/10.1007/s11249-016-0768-6
85. Chromik, R.R., Strauss, H.W., Scharf, T.W.: Materials phenomena revealed by in situ tribometry. Jom **64**, 35–43 (2012). https://doi.org/10.1007/s11837-011-0229-5
86. Cann, P.M., Spikes, H.A.: In lubro studies of lubricants in EHD contacts using FTIR absorption spectroscopy. Tribol. Trans. **34**, 248–256 (1991). https://doi.org/10.1080/10402009108982033
87. Wan, G.T.Y., Spikes, H.A.: The behavior of suspended solid particles in rolling and sliding elastohydrodynamic contacts. Tribol. Trans. **31**, 12–21 (1988). https://doi.org/10.1080/10402008808981793
88. Cann, P.M., Spikes, H.A., Hutchinson, J.: The development of a spacer layer imaging method (slim) for mapping elastohydrodynamic contacts. Tribol. Trans. **39**, 915–921 (1996). https://doi.org/10.1080/10402009608983612
89. Johnston, G.J., Wayte, R., Spikes, H.A.: The measurement and study of very thin lubricant films in concentrated contacts. Tribol. Trans. **34**, 187–194 (1991). https://doi.org/10.1080/10402009108982026
90. Murashima, M., Imaizumi, Y., Murase, R., Umehara, N., Tokoroyama, T., Saito, T., et al.: Active friction control in lubrication condition using novel metal morphing surface. Tribol. Int. **156**, 106827-1–106829 (2021). https://doi.org/10.1016/j.triboint.2020.106827
91. Nishimura, H., Umehara, N., Kousaka, H., Murashima, M.: Clarification of effect of transformed layer and oil film on low friction coefficient of CNx coating in PAO oil lubrication by in-situ observation of friction area with reflectance spectroscopy. Tribol. Int. **113**, 383–388 (2017). https://doi.org/10.1016/j.triboint.2016.10.029
92. Maruyama, T., Nakano, K.: In situ quantification of oil film formation and breakdown in EHD contacts. Tribol. Trans. **61**, 1057–1066 (2018). https://doi.org/10.1080/10402004.2018.1468519
93. Maruyama, T., Maeda, M., Nakano, K.: Lubrication condition monitoring of practical ball bearings by electrical impedance method. Tribol. Online **14**, 327–338 (2019). https://doi.org/10.2474/trol.14.327
94. Ohara, K., Hanyuda, K., Kawamura, Y., Omura, K., Kameda, I., Umehara, N., et al.: Analysis of wear track on DLC coatings after sliding with MoDTC-containing lubricants. Tribol. Online **12**, 110–116 (2017). https://doi.org/10.2474/trol.12.110
95. Nishimura, H., Umehara, N., Kousaka, H., Tokoroyama, T.: Clarification of relationship between friction coefficient and transformed layer of CNx coating by in-situ spectroscopic analysis. Tribol. Int. **93**, 660–665 (2016). https://doi.org/10.1016/j.triboint.2014.12.015
96. Hashizume, N., Murashima, M., Umehara, N., Tokoroyama, T., Lee, W.-Y.: In situ observation of the formation of

MoDTC-derived tribofilm on a ta-C coating using reflectance spectroscopy and its effects on friction. Tribol. Int. **162**, 107128 (2021). https://doi.org/10.1016/j.triboint.2021.107128
97. Okamoto, T., Umehara, N., Tokoroyama, T., Murashima, M.: The clarification of low friction mechanism in base oil lubrication of ta-CNx coating by in-situ observation with reflectance spectroscopy. Trans. JSME (in Japanese) **85**, 19–00071 (2019). https://doi.org/10.1299/transjsme.19-00071
98. Gangopadhyay, A., Liu, Z., Simko, S.J., Peczonczyk, S.L., Cuthbert, J.B., Hock, E.D., et al.: Friction and wear reduction mechanism of polyalkylene glycol-based engine oils. Tribol. Trans. **61**, 621–631 (2018). https://doi.org/10.1080/10402004.2017.1381286
99. Neumann, A.W.: Applied Surface Thermodynamics. CRC Press, Boca Raton (1996)
100. K. Stana-Kleinschek VR. Electrokinetic Phenomena. Proceedings of the International Conference, 1998, p. 10.
101. Myers, D.: Surfaces, Interfaces and Colloids — Principles and Applications, 2nd edn. Wiley-VCH, New York (1999)
102. Gu, H., Wang, C., Gong, S., Mei, Y., Li, H., Ma, W.: Investigation on contact angle measurement methods and wettability transition of porous surfaces. Surf. Coat. Technol. **292**, 72–77 (2016). https://doi.org/10.1016/j.surfcoat.2016.03.014
103. Owens, D.K., Wendt, R.C.: Estimation of The Surface Energy of Polymers. J. Appl. Polym. Sci. **13**, 1741–1747 (1969)
104. Nishimura, H., Umehara, N., Kousaka, H., Deng, X.: The clarification of low friction mechanism for hydrogenated amorphous carbon by in-situ observation of frictional area. Tribol. Online **11**, 341–347 (2016). https://doi.org/10.2474/trol.11.341
105. Fujiwara H. Spectroscopic Ellipsometry. Tokyo: Maruzen Publishing Co. (in Japanese); 2003.
106. Hamrock BJ, Dowson D (1976) Isothermal Elastohydrodynamic Lubrication of Point Contacts - 3. Fully Flooded Results. American Society of Mechanical Engineers (Paper).
107. Walton, O.R.: Review of adhesion fundamentals for micron-scale particles. KONA Powder Part. J. **26**, 129–141 (2008). https://doi.org/10.14356/kona.2008012
108. Nase, S.T., Vargas, W.L., Abatan, A.A., McCarthy, J.J.: Discrete characterization tools for cohesive granular material. Powder Technol. **116**, 214–223 (2001). https://doi.org/10.1016/S0032-5910(00)00398-3
109. Thornton, C., Ning, Z.: A theoretical model for the stick/bounce behaviour of adhesive, elastic- plastic spheres. Powder Technol. **99**, 154–162 (1998). https://doi.org/10.1016/S0032-5910(98)00099-0
110. Seville, J.P.K., Willett, C.D., Knight, P.C.: Interparticle forces in fluidisation: a review. Powder Technol. **113**, 261–268 (2000). https://doi.org/10.1016/S0032-5910(00)00309-0
111. Murashima, M., Umehara, N., Kousaka, H., Deng, X.: Effect of electric field on adhesion of thermoplastic resin against steel plate. Tribol. Online **12**, 42–48 (2017). https://doi.org/10.2474/trol.12.42
112. Murashima, M., Hojo, K., Ito, S., Umehara, N., Tokoroyama, T., Takahashi, T., et al.: Nanotextured Mold surface with DLC coating for reduction in residual ceramic particles. Langmuir **37**, 3563–3574 (2021). https://doi.org/10.1021/acs.langmuir.0c03435
113. Lundgren, S.M., Ruths, M., Danerlöv, K., Persson, K.: Effects of unsaturation on film structure and friction of fatty acids in a model base oil. J. Colloid Interface Sci. **326**, 530–536 (2008). https://doi.org/10.1016/j.jcis.2008.05.068
114. Doig, M., Warrens, C.P., Camp, P.J.: Structure and friction of stearic acid and oleic acid films adsorbed on iron oxide surfaces in squalane. Langmuir **30**, 186–195 (2014). https://doi.org/10.1021/la404024v
115. Wood, M.H., Casford, M.T., Steitz, R., Zarbakhsh, A., Welbourn, R.J.L., Clarke, S.M.: Comparative adsorption of saturated and unsaturated fatty acids at the iron oxide/oil interface. Langmuir **32**, 534–540 (2016). https://doi.org/10.1021/acs.langmuir.5b04435
116. Yoshino, A., Kikuyama, K., Miyata, K., Yamashita, S.: Hydrodynamic Engineering Excercises. Kyoritsu Publishing Co., Tokyo (1989)
117. Yamamoto Y, Kamata M. Tribology. Tokyo: Ohmsha Co.; 1998.
118. Barus, C.: Isothermals, isopiestics and isometrics relative to viscosity. Am. J. Sci. **s3–45**, 87–96 (1893). https://doi.org/10.2475/ajs.s3-45.266.87
119. Hirata, K., Murashima, M., Umehara, N., Tokoroyama, T., Hashizume, N., Lee, W.Y., et al.: Clarification of the effects of adsorption films of ester-blended oil on friction by in situ reflectance spectroscopy. Tribol. Int. (2023). https://doi.org/10.1016/j.triboint.2023.108718
120. Peeters, S., Barlini, A., Jain, J., Gosvami, N.N., Righi, M.C.: Adsorption and decomposition of ZDDP on lightweight metallic substrates: Ab initio and experimental insights. Appl. Surf. Sci. **600**, 153947 (2022). https://doi.org/10.1016/j.apsusc.2022.153947